Journal of Catalysis 265 (2009) 54–62

Contents lists available at ScienceDirect

Journal of Catalysis

journal homepage: www.elsevier.com/locate/jcat

Oxidative dehydrogenation (ODH) of ethane with O_2 as oxidant on selected transition metal-loaded zeolites

Xufeng Lin, Cathleen A. Hoel, Wolfgang M.H. Sachtler, Kenneth R. Poeppelmeier *, Eric Weitz *

Department of Chemistry and Institute for Catalysis in Energy Processes, Northwestern University, Evanston, IL 60208, USA

ARTICLE INFO

Article history:
Received 26 January 2009
Revised 10 April 2009
Accepted 14 April 2009
Available online 17 May 2009

Keywords:
Oxidative dehydrogenation
Ethane
Ethylene productivity and selectivity
Transition metal Y Zeolite

ABSTRACT

Ni-, Cu-, and Fe-loaded acidic and basic Y zeolites were synthesized, and their catalytic properties for oxidative dehydrogenation of ethane (ODHE) to ethylene were characterized. Acidic Ni-loaded Y zeolite exhibits an ethylene productivity of up to 1.08 $g_{C_2H_4}\ g_{cat}^{-1}\ h^{-1}$ with a selectivity of ~75%. Acidic Cu- and Fe-loaded Y zeolites have an ethylene productivity of up to 0.37 $g_{C_2H_4}\ g_{cat}^{-1}\ h^{-1}$ and a selectivity of ~50%. For the same metal, the acidity of the zeolite favors both ODHE productivity and ethylene selectivity. Extended X-ray absorption fine structure (EXAFS) studies show that Ni, present in particles on Ni/HY during the ODHE catalytic process, contains both Ni–Ni and Ni–O bonds, and that the ratio of oxidized Ni versus metallic Ni increases with the temperature. The insights these studies provide into the ODHE reaction mechanism are discussed.

1. Introduction

The demand for light olefins, which are feed stocks for the synthesis of a wide variety of chemicals, is increasing. The principal current method for the production of ethylene is steam cracking (usually carried out at $T > 800$ °C), which is energy intensive. Besides the high energy cost, other drawbacks include significant side reactions and catalyst deactivation owing to carbon deposition. Oxidative dehydrogenation (ODH) of light paraffins with O_2 is a potential alternative for the production of light olefins. ODH has the potential to overcome the major drawbacks of the principal current method by operating at a much lower temperature, since such ODH reactions are exothermic. However, in the ODH processes it is difficult to avoid over-oxidation of the partially oxidized products to undesired carbon oxides (CO_x). The key issue for the oxidative dehydrogenation of light alkanes is to improve both the activity and selectivity of catalysts [1,2]. As an example, in the case of the ODH of ethane (ODHE), for a catalyst to be viewed as promising for industrial implementation, it should have an ethylene productivity greater than 1 $g_{C_2H_4}\ g_{cat}^{-1}\ h^{-1}$ [1]. In the literature, V [3–18], Mo [19–25], and Pt [26–31] based catalysts and V–Mo mixed oxides [32–38] are the most widely studied transition metal catalysts for ODHE. In contrast, the more abundant transition metals, such as Fe, Cu, and Ni, have been less studied and have generally yielded less promising results [39–45]. For example, unsupported Fe_2O_3, Co_2O_3, and NiO have been examined as ODHE catalysts by Schuurman et al. [45] and 1% ethane conversion was achieved at the relatively low temperature of ~500 K. Zhang et al. [43,44] reported a NiO/Al_2O_3 catalyst with good activity and selectivity for ODHE at relatively low temperatures (350 to 450 °C). NiO-loaded high surface area MgO was examined for ODHE at 600 °C by Nakamura and co-workers [40]; a C_2H_6 conversion of 68.8% and a C_2H_4 selectivity of 52.8% were achieved. These results also suggest that the catalyst support can affect ODHE performance.

Zeolites, which have molecular scale pore/cage sizes, provide a good template for the fabrication of supported catalysts. Importantly, the catalytic properties of zeolites can potentially be tuned by the type of zeolite employed, the nature of the active metal, the Si/Al ratio, and the acid–base character of the zeolite. As such, efforts have been made to utilize metal-loaded zeolites as catalysts for the selective oxidation of hydrocarbons. For example, Fe/MFI is an effective catalyst for the one-step oxidation of benzene to phenol [46–54], as well as for the oxidative dehydrogenation of ethane and propane [55–61] with N_2O as the oxidant. However, there are only a few reports using transition metal-loaded zeolites as catalysts for ODHE with O_2 as the oxidant. The latter studies mainly employed V [12,15,16], a "traditional" choice for oxidative dehydrogenation, as the active metal.

Transition metal-loaded zeolites can be prepared by several methods including: wet or solid ion exchange, incipient wetness impregnation, chemical vapor deposition, and direct hydrothermal synthesis [62]. When a metal ion is reduced by H_2, a Brønsted acid site is created to maintain the electric neutrality of the zeolite [63,64]. Additionally, reduced metal atoms could migrate to form

* Corresponding authors. Fax: +1 847 491 7713 (E. Weitz).
E-mail address: Weitz@northwestern.edu (E. Weitz).

0021-9517/$ - see front matter © 2009 Elsevier Inc. All rights reserved.
doi:10.1016/j.jcat.2009.04.007

metal particles [63] that are thermodynamically favored over isolated metal atoms. Both metal particles and Brønsted acid sites can be catalytically active and can be operated synergistically. For example, unusually high hydrogenation activity has been found for Pt particles in Y zeolite cages, which is ascribed to the electron deficiency of the Pt particles induced by zeolite protons [65]. If the Brønsted acid site is not favorable for the reaction of interest, it can be removed by ion exchange with a solution of alkali or alkaline earth ions [66].

In this paper, the preparation, characterization, and investigation of the catalytic properties of the acidic and basic forms of Ni-, Cu-, and Fe-loaded Y zeolites for the oxidative dehydrogenation of ethane to ethylene (ODHE) are reported. Ni-loaded acidic Y zeolite has a C_2H_4 productivity $> 1\ g_{C_2H_4}\ g_{cat}^{-1}\ h^{-1}$, with an ethylene selectivity of ~75%. The acidity of the zeolite favors both the conversion to ethylene and the selectivity of the process. The implications of this work with regard to proposed ODHE reaction mechanisms are discussed.

2. Experimental

2.1. Catalyst preparation

Ion exchanges were performed by mixing 200 ml of 0.1 mol/L metal sulfate ($FeSO_4$, $CuSO_4$, or $NiSO_4$) solution with 6 g of Y zeolite (Sodium-form, Si/Al = 2.4, Aldrich). The mixture was then stirred for 6 h at 88 °C. After filtering, the transition metal-loaded zeolites were washed with large amounts of water and dried at 110 °C. The resulting powder was reduced in a H_2 flow in a U-tube reactor maintained at 500 °C for 12 h. Metal ions in the zeolite cage could be reduced to their zero-valent state as a result of the reaction in Eq. (1):

$$M^{n+}\text{-zeol} + n/2H_2 \rightarrow M + nH^{+}\text{-zeol} \quad (1)$$

Consistent with this expectation, a color change was observed after H_2 reduction: from green to black for Ni, from blue to pink for Cu, and from light yellow to dark gray for Fe. The product obtained from treatment with H_2 was denoted as M/HY. Transition metal-loaded basic zeolites were obtained by a subsequent ion-exchange step carried out on M/HY. M/HY (3 g) was mixed with 100 ml of 0.5 mol/L KOH solution, and the slurry was stirred at 80 °C for 10 h. The resulting zeolites are denoted as M/KY. All M/HY and M/KY zeolites were calcined at 615 °C in a He or Ar flow for 4 h before use. The H form of Y zeolite (HY) was prepared by a threefold ion exchange of NaY with 0.1 M NH_4NO_3 to make NH_4Y [67], followed by calcining in an Ar flow at 500 °C for 4 h. All chemicals were of analytical purity, and de-ionized water was used in all solutions.

2.2. Catalyst characterization

The chemical composition of the as-prepared metal-loaded zeolites was determined by inductively coupled plasma atomic emission spectroscopy (ICP-AES). An HF/HNO_3 solution was used to dissolve the zeolite samples for ICP analysis. X-ray powder diffraction (XRD) patterns were recorded at room temperature on a Rigaku diffractometer (Cu K_α radiation, Ni filter, 40 kV, 20 mA, $2\theta = 10°$ to 70°, 0.05° step size, and 1 s count time). Infrared spectra were collected with a Thermo Nicolet Nexus 870 FTIR spectrometer. Temperature programmed desorptions (TPDs) of NH_3 and C_2H_4 were performed with a computer controlled reactor (AMI-200, Altamira) with a thermal conductivity detector (TCD).

X-ray absorption measurements at the Ni (8333 eV) and Cu (8992 eV) *K*-edges were carried out at the DND-CAT (sector 5 beamline 5-BMD) at the Advanced Photon Source (APS) at Argonne National Laboratory. The 100 mA beam ran through a Si(1 1 1) double-crystal monochromator detuned to 70% of the maximum counts to reject harmonics. A thin layer of the sample powder was spread onto clear adhesive tape. The samples were measured up to $k = 16\ Å^{-1}$ in fluorescence mode using a Lytle cell [68] filled with Xe. Each measurement included a Ni or Cu foil as an energy reference and standard. The data were analyzed with WinXAS 2.1 to obtain the normalized $\chi(k)$ EXAFS spectra and the respective Fourier transformed $[k^{2^*}\chi(k)]$ spectra ($k = 2.0$ to $10.0\ Å^{-1}$). Athena [69] was used to determine the compositions of the different metal oxidation states via linear combinatorial fitting of the $[k^{2^*}\chi(k)]$ spectra.

2.3. Catalytic reaction tests

The ODH of ethane was carried out in a tubular quartz microreactor operating at atmospheric pressure. Typically, 100 mg of catalyst was mixed with 1 g of quartz particles in order to avoid catalytic "hot spots". The reaction feed contained 9.7 ml/min C_2H_6 (Airgas, purity > 99.99%), 3.3 ml/min O_2 (Airgas, purity > 99.98%), and 62 ml/min He (Airgas, purity > 99.999%) at 22 °C. The reaction products were analyzed with an HP 5890 series II gas chromatograph equipped with a TCD. A Porapak Q 80/100 column was used to separate CO_2, C_2H_4, and C_2H_6 and a molecular sieve 5 A column was used to separate O_2 and CO. The ethane conversion and the ethylene selectivity were calculated on the basis of carbon mass with a total mass balance of between 95% and 100%. The homogenous reaction of ethane and its reaction over quartz did not lead to a measurable conversion of ethane at 550 °C, with less than 0.5% conversion at 600 °C. Tests of ethylene oxidation using a C_2H_4 (Matheson, purity > 99.99%) flow rate of 4 ml/min and an O_2 flow rate of 3.3 ml/min were also carried on Ni/HY and Ni/KY catalysts. The conversion of C_2H_6 ($X_{C_2H_6}$) and the selectivity ($S_{C_2H_4}$) of C_2H_4 are based on the carbon mass balance, and were calculated by the following equations:

$$X_{C_2H_6} = \frac{[CO] + [CO_2] + 2[C_2H_4]}{2[C_2H_6]_{reactant}} \times 100\%$$

$$S_{C_2H_4} = \frac{2[C_2H_4]}{[CO] + [CO_2] + 2[C_2H_4]} \times 100\%$$

The productivity of C_2H_4 is given by $N_{C_2H_6} * X_{C_2H_6} * S_{C_2H_4} * 28/W_{catalyst}$, where $N_{C_2H_6}$ is the flow rate of C_2H_6 in mol/h, 28 (g/mol) is the molar mass of C_2H_4, and $W_{catalyst}$ is the weight of catalyst used.

3. Results and discussion

3.1. Characterization of as-prepared M/HY and M/KY catalysts (M = Ni, Cu, and Fe)

The XRD results in Fig. 1 show that the as-prepared Ni-loaded acidic and basic Y zeolites exhibit diffraction patterns that are similar to those of the NaY starting material (i.e. they are all lacking the metal or oxide phase contribution). The absence of peaks due to the metal or metal oxide in metal-loaded zeolites was also noted by Zhan et al. [70] for RuO_2 encaged LTA zeolite. This could be due to the fact that the metal/metal oxide particles in the zeolite are smaller than the XRD detection limit. The Cu- and Fe-loaded Y zeolites give XRD patterns that are similar to those for Ni-loaded Y zeolites. These XRD results indicate that the zeolitic framework remains intact during ion exchange and the H_2 reduction process. This is further confirmed by the infrared spectra of the M/HY and M/KY zeolites, which are all similar to the spectrum of NaY (not shown here). The ICP-AES results listed in Table 1 show that a single ion-exchange step leads to a M/Al ratio of ~35%. The second ion-exchange step, with KOH solution, is effective for the removal

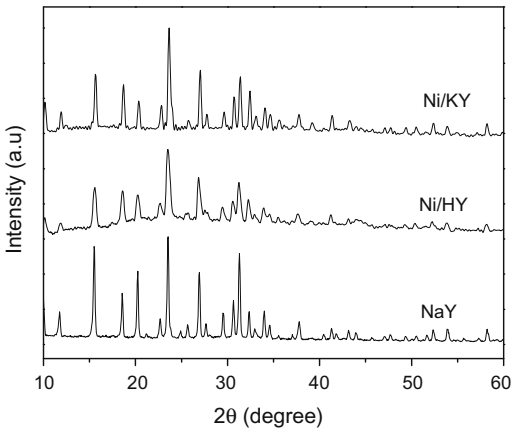

Fig. 1. X-ray diffraction patterns of Ni-loaded Y zeolite.

Table 1
Chemical composition of metal (M = Ni, Cu, and Fe) loaded Y zeolite measured by ICP-AES. The metal to Al ratios are calculated based on the molar concentration, i.e. the [M]/[Al] ratio in the solution of the dissolved samples.

	Si/Al	M/Al	Na/Al	K/Al
NaY			0.82	
HY			0.09	
Ni/HY		0.36	0.33	
Ni/KY	2.4	0.37	0.16	0.83
Cu/HY		0.37	0.33	
Cu/KY		0.36	0.16	0.81
Fe/HY		0.37	0.30	
Fe/KY		0.34	0.18	0.85

of the acidic zeolite site, as evidence by a K/Al ratio of ~83% and a [K + Na]/[Al] ratio of ~1.

The ICP-AES result does not give the ratio of Brønsted acid sites to Al ionic sites (i.e. $[H^+]/[Al]$) for metal-loaded acidic Y zeolite. Thus, NH_3-TPD was carried out on both Ni/HY and Ni/KY to obtain the $[H^+]/[Al]$ value for Ni/HY, based on the assumption that the $[H^+]/[Al]$ for Ni/KY is 0 (since [K + Na]/[Al] > 0.99 in Ni/KY). NaY and HY were used as reference materials since the number of Brønsted acid sites is readily determinable (*vide supra*) for these zeolites. Fig. 2 shows the NH_3-TPD curves for Ni-loaded acidic and basic Y zeolites as well as those for NaY and HY. The ratio of Brønsted acid sites to Al sites is calculated from the following equation:

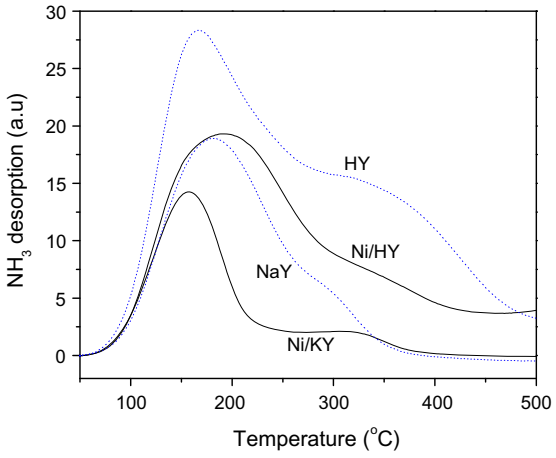

Fig. 2. NH_3-TPD of 0.100 g: (a) Ni/HY, (b) Ni/KY, (c) HY, and (d) NaY as indicated.

$$(H/Al)_{Ni/HY} = \frac{A_{NiHY}/n^{Al}_{NiHY} - A_{Ni/KY}/n^{Al}_{NiKY}}{(A_{HY}/n^{Al}_{HY} - A_{NaY}/n^{Al}_{NaY}) * (0.91 - 0.18)},$$

where A represents the area of the NH_3 desorption peak between 50 and 500 °C, n^{Al} is the number of moles of Al, and 0.91 and 0.18 are the H/Al values for NH_4Y and NaY, respectively. These two values as deduced from the ICP results (Table 1) show that the Na/Al values for these sample are 0.09 and 0.82, respectively. The above-mentioned equation gives a $(H/Al)_{Ni/HY}$ of 0.65, which is consistent with the ICP result for $(Na/Al)_{Ni/HY}$ of 0.33 (the overall number of cations is equal to the number of Al ions in the zeolite).

3.2. ODH of ethane on M/HY and M/KY (M = Ni, Cu, and Fe)

The performance of catalysts for the ODH reactions depends on a variety of factors including the nature of the metal, type of support, surface acidity, accessible surface area, dispersion of the metal, gas space velocity, alkane/O_2 ratio, and diluent gas. The present work focuses on the comparison of results for different metals and different zeolite acidities. The ODH of ethane over selected transition metal-loaded Y zeolites led to predominantly C_2H_4, CO_2, and small amounts of CO. Other hydrocarbons were not observed. Based on the stoichiometry of the reaction: $C_2H_6 + 1/2O_2 = C_2H_4 + H_2O$, full conversion of O_2, and complete C_2H_4 selectivity will lead to a maximum C_2H_6 conversion of $2 \times 3.3/9.7 = 68.0\%$. However, in this work, the conversion of O_2 never reached 100%.

Table 2 lists the ethylene productivity for the ODH reaction of ethane over 0.1 g of each of Ni/HY, Ni/KY, Cu/HY, and Cu/KY, and 0.2 g of each of Fe/HY and Fe/KY catalysts between 450 and 600 °C. Ni/HY gives the best C_2H_4 selectivity and productivity (up to 1.08 $g_{(C_2H_4)}\ g^{-1}_{(cat)} * h^{-1}$) among all the catalysts tested in this study. The C_2H_6 conversion is 1.1% higher at 450 °C for 0.1 g Ni/HY than 0.1 g Ni/KY, and is 7.6% higher at 600 °C (see Fig. 3a and b). The C_2H_4 selectivity increases with temperature from 66% at 450 °C to ~75% at 550 to 600 °C for Ni/HY (Fig. 4a). As a comparison, the C_2H_4 selectivity increases with temperature from 58% at 450 °C to ~73% at 550 to 600 °C for Ni/KY (Fig. 4b). These data indicate that Ni/HY has a higher ODHE activity and a higher C_2H_4 selectivity than Ni/KY.

Although this work did not examine the effect of the support on the catalytic performance, it is interesting to compare the present results with those in the literature for supported and unsupported Group VIII metal oxides. The ethylene selectivity has been reported as 50% to 60% for unsupported NiO between 475 and 600 K (increasing with temperature) with a C_2H_6 conversion of 1–18% [45] (the GSHV of ethane is 2.8 $L/h^* g_{cat}$ in reference 45, and 5.8 $L/h^* g_{cat}$ in this work). The trend for C_2H_4 selectivity with temperature on NiO is the same as that for the Ni-loaded Y zeolites used in this work. ODHE reactions were carried out at relatively low temperatures (350 to 450 °C) for NiO with alumina supports of differing surface areas [43]. The C_2H_4 selectivity ranged from 46.9% to 72.5% with conversions from 43.3% to 59.1% at 450 °C (the GSHV of ethane is 0.34 $L/h^* g_{cat}$). A higher C_2H_4 yield was obtained on the catalysts with the higher pore volume/surface area ratios. A C_2H_6 (GSHV = 15 $L/h^* g_{cat}$) conversion of 68.8% and a C_2H_4 selectivity of 52.8% were obtained on NiO dispersed on high surface area MgO at 600 °C [40]. The C_2H_4 selectivity decreases with temperature for NiO/alumina, which is different than the results for bulk NiO [45], NiO/MgO [40], and Ni/HY and Ni/KY reported in this work.

Cu- and Fe-loaded Y zeolites are less active and less selective for ethylene (Figs. 5 and 6, respectively) when compared to Ni-loaded Y zeolites. The ODH activity of a metal-loaded Y zeolite is greater for Ni than for Fe, which follows the same order of ODH activity on the unsupported Fe and Ni oxides [45]. To our knowledge, there are no prior reports of ODHE reactions on Cu. The C_2H_4 productivity at 450 °C for Cu/HY (0.10) is close to that for Ni/HY (0.11), while

Table 2
Data for the productivity of ethylene (in $g_{C_2H_4}\ g_{cat}^{-1}\ h^{-1}$) from the ethane ODH reaction catalyzed by transition metal (M = Ni, Cu, and Fe) loaded acidic and basic zeolites, the selectivity (S) and the yield (Y), where the yield is the product of the $S \cdot$ conversion (where the conversion is taken from Figs. 3, 5 and 6), are included.

Catalyst	W/F_{C2H6} (g_{cat} s/ml)	450 °C			600 °C		
		$S_{C_2H_4}$ (%)	$Y_{C_2H_4}$ (%)	Productivity	$S_{C_2H_4}$ (%)	$Y_{C_2H_4}$ (%)	Productivity
Ni/HY	0.62	66.3	1.7	0.11	74.5	15.8	1.08
Ni/KY	0.62	58.1	0.9	0.058	72.9	10.0	0.67
Cu/HY	0.62	56.8	1.5	0.10	45.3	5.5	0.37
Cu/KY	0.62	47.8	1.1	0.073	36.2	4.4	0.30
Fe/HY	1.24	52.7	2.9	0.096	42.8	7.5	0.25
Fe/KY	1.24	6.3	0.3	0.010	37.6	3.7	0.12

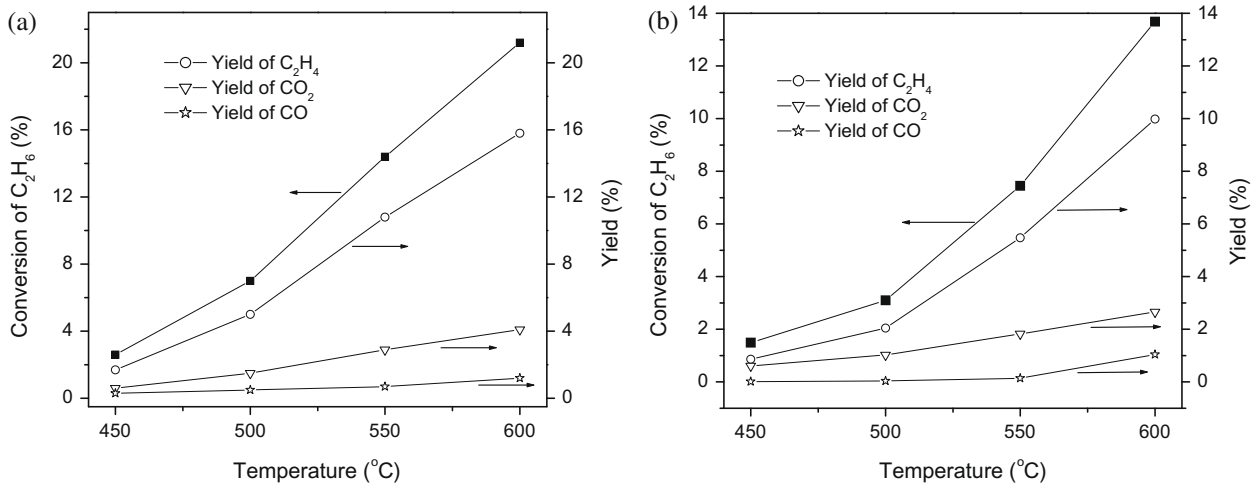

Fig. 3. Temperature dependence of the conversion of ethane and the yield of ethylene, CO_2, and CO for the ODH of ethane on 0.1 g Ni/HY (a) and 0.1 g Ni/KY catalysts (b).

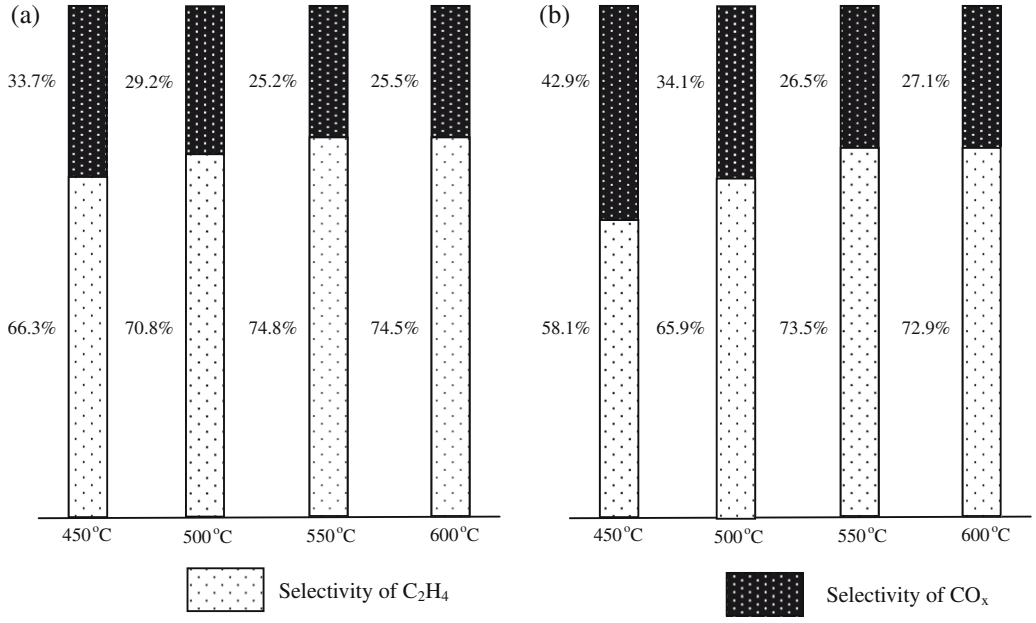

Fig. 4. Temperature dependence of the selectivity for ethylene and CO_x in the ODH of ethane using (a) 0.1 g Ni/HY and (b) 0.1 g Ni/KY.

at higher temperatures (i.e. ~600 °C) the C_2H_4 productivity is far poorer for Cu/HY than for Ni/HY. Similarly, Fe/HY has an ethylene productivity that is comparable to that for Cu/HY at 450 °C but the productivity is substantially lower at 600 °C. On the other hand, both higher ethane conversion and selectivity were observed on acidic zeolites than on basic zeolites (compare Fig. 5a and b for Cu, and Fig. 6a and b for Fe). Both Cu/HY and Fe/HY give a C_2H_4 selectivity of ~50% over the temperature range from 450 to ~600 °C, with the selectivity decreasing slightly with temperature. For Cu/KY, the C_2H_4 selectivity decreases from 48% at 450 °C to 36% at 600 °C. The C_2H_4 selectivity of Fe/KY is the poorest of any of the catalysts examined in this work, especially in the lower tempera-

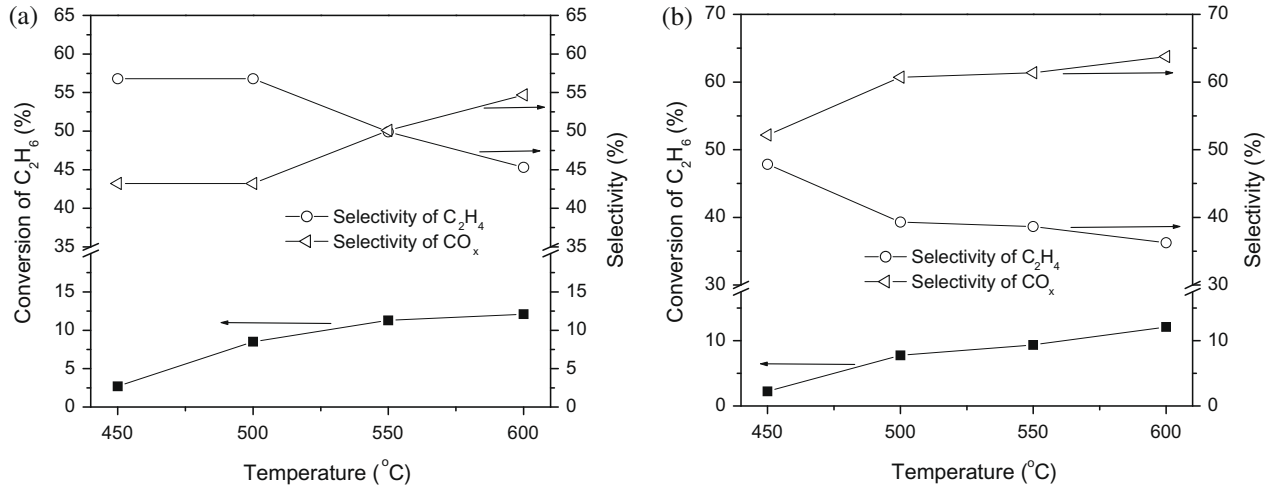

Fig. 5. Temperature dependence of C_2H_6 conversion and C_2H_4 and CO_x selectivities using (a) 0.1 g Cu/HY and (b) 0.1 g Cu/KY.

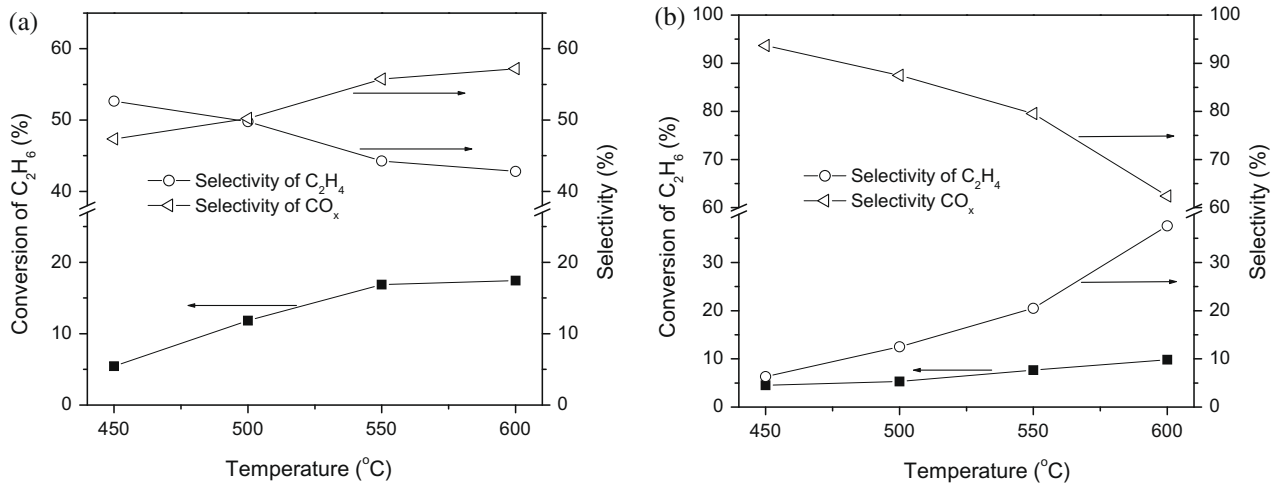

Fig. 6. Temperature dependence of C_2H_6 conversion and C_2H_4 and CO_x selectivities using (a) 0.2 g Fe/HY and (b) 0.2 g Fe/KY.

ture region. For example, the C_2H_4 selectivity of Fe/KY is only 6.3% at 450 °C and increases to 37.6% at 600 °C. The C_2H_4 selectivity was between 25 and 50% (decreasing with temperature) for ODHE reactions catalyzed by unsupported Fe_2O_3 which were run between 543 and 703 K at a conversion of 1 -11% [45]. The profile for the temperature dependence for C_2H_4 selectivity differs among Fe_2O_3, Fe/HY (decreasing slightly with temperature), and Fe/KY (mildly increasing with temperature).

Though zeolite acidity is utilized for paraffin cracking, alkene oligomerization, etc. [71], it has seldom been utilized for the oxidative dehydrogenation of light alkanes. However, it has been noted [2] that the selectivity for alkene production can be controlled by the acid–base character of a catalyst, which can be modified by appropriate additives or supports. For example, MoO_x on supports with high surface acidity, e.g. Al_2O_3, displays higher C_2H_4 selectivity than on supports with lower surface acidity, e.g. TiO_2 [19]. Kao et al [72] have reported that ethane ODH rates over vanadium oxides are enhanced by the presence of acidic sites. One of the advantages of zeolite supports is the relative ease with which the type and amount of exchanged ion can be controlled, and thus used to "tune" catalytic performance. The results of this section suggest that it would be interesting to study the effect of exchanged ions on metal-loaded zeolites on the ODH of light alkanes in addition to ethane.

3.3. Ethane oxidation vs. ethylene oxidation on Ni/HY and Ni/KY

A comparison of ethane conversion and selectivity obtained with Ni-, Cu-, and Fe-loaded acidic and basic Y zeolites (see Figs. 3–6) demonstrates that zeolite acidity favors both C_2H_6 conversion and C_2H_4 selectivity. The remainder of this paper is devoted to a discussion of the ODHE kinetics, reaction mechanism, and catalyst structure, and focuses on Ni-loaded Y zeolite, which is the most promising of the catalysts for ODHE studied in this work. According to the generally accepted scheme for ethane ODH [73], depicted in Eq. (2), C_2H_4 is an intermediate in one of the pathways for the total oxidation of C_2H_6. Therefore, the rate constants, k_1 and k_2, determine the ODHE activity, and the ratios of rate constants, k_1/k_2 and k_1/k_3, determine the C_2H_4 selectivity. Smaller values for k_3/k_1 and k_2/k_1 lead to better selectivity. Thus, a comparison of the rates for the oxidation of both C_2H_6 and C_2H_4 on Ni/HY and Ni/KY can provide information about the trends in these ratios of rate constants.

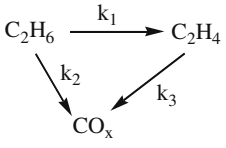

(2)

Fig. 7a and b depict the temperature dependence of the turnover frequency (TOF) for ethane and ethylene oxidation, respectively, on the Ni/HY and Ni/KY catalysts. Fig. 8 gives the ratio of the TOF for ethane oxidation and ethylene oxidation on both catalysts. TOF is calculated by

$$\mathrm{TOF} = \frac{\text{Number of moles of } C_2H_6 \text{ or } C_2H_4 \text{ reacted in one second}}{\text{Number of moles of Ni in the catalyst}}$$

Since not all the Ni in the zeolite will be equally accessible to the reactants, the TOF number reported here should be viewed as a lower limit. Since the reaction was run in a fixed-bed flow reactor, it is reasonable to assume that the concentration of the flow did not change after a steady state was achieved. TOF is therefore expected to be proportional to the reaction rate, which is proportional to k. Thus, the profiles shown in Fig. 8 for the TOF can be taken as indicators of the trend for $k_3/(k_1 + k_2)$ *vs.* T for each catalyst. Inspection of Fig. 7a and b shows that zeolite acidity favors $(k_1 + k_2)$, and disfavors k_3. Fig. 8 indicates that, on both catalysts, k_3 increases with temperature more slowly than $(k_1 + k_2)$. This is consistent with an increase in the ethylene selectivity over the temperature range from 450 to 600 °C. On the other hand, the ratio $k_3/(k_1 + k_2)$ is larger for Ni/KY than for Ni/HY, and the difference in this ratio for Ni/KY relative to Ni/HY becomes smaller with increasing temperature. This trend is consistent with the observation that Ni/HY has a higher C_2H_4 selectivity than Ni/KY, especially at lower temperature. Information on the magnitude of the ratio of k_1/k_2 cannot be obtained from the data shown in Figs. 7 and 8, i.e., the contribution to the C_2H_6 oxidation via the pathway (the left branch in Eq. (2)) that does not involve C_2H_4 as the intermediate.

Since a reaction product must remain on the catalyst surface to undergo subsequent heterogeneous reactions, it is reasonable to expect that faster desorption of C_2H_4 from the catalyst surface will lead to a lower probability for further oxidation to undesirable CO_x products. Thus, a comparison made among the rates of desorption of C_2H_4 on metal-loaded both acidic and basic zeolites is useful. Fig. 9 shows the temperature programmed desorption profiles for ethylene on both H_2-treated Ni/HY and Ni/KY. The C_2H_4-TPD curve for Ni/HY exhibits a large peak at 365 °C and a smaller peak at 565 °C. By comparison, the TPD curve for Ni/KY exhibits a large peak at a much lower temperature (180 °C), and the lower intensity higher temperature peak is also at lower temperature relative to Ni/HY. Fig. 9 shows that Ni/HY tends to adsorb larger amounts of C_2H_4 than Ni/KY, and that the desorption of C_2H_4 from Ni/HY takes place at a higher temperature than that from Ni/KY.

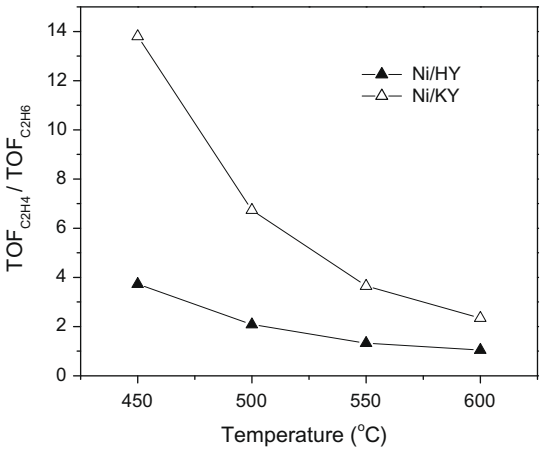

Fig. 8. The ratio of the turnover frequency for ethylene oxidation to that for ethane oxidation on Ni/HY (solid triangles) and Ni/KY (open triangles) derived from the data shown in Fig. 7.

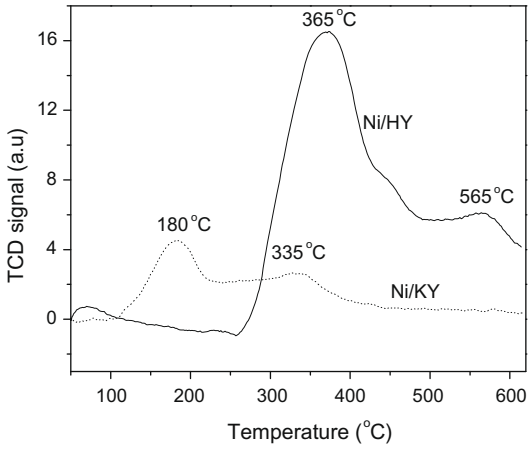

Fig. 9. C_2H_4-TPD profiles of (a) 0.112 g Ni/HY (solid line) and (b) 0.114 g Ni/KY (dotted line). Both samples were pretreated in a H_2 flow at 500 °C for 4 h.

In addition, we note that some coke formation was observed after the catalytic test, however, this was a relatively minor reaction channel relative to those indicated by $k_1 - k_3$, as evidenced

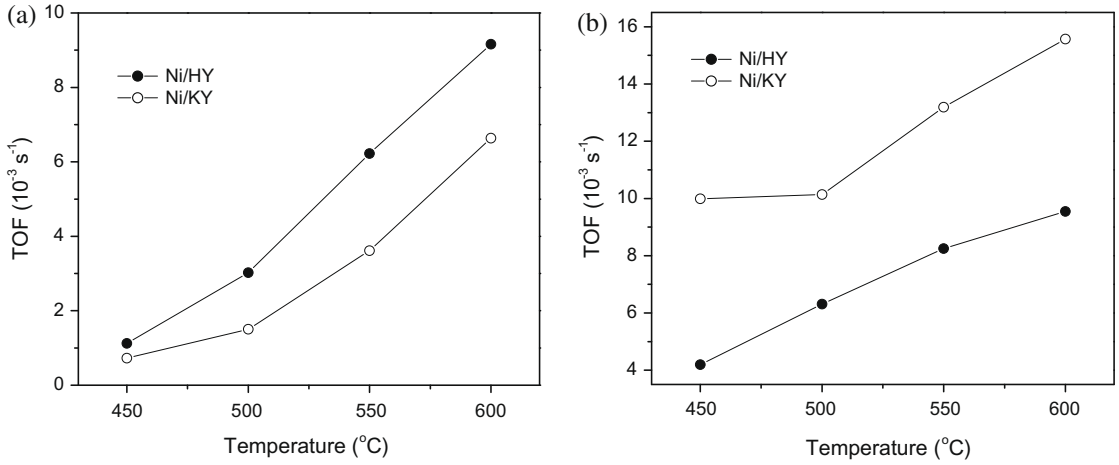

Fig. 7. Temperature dependence of the turnover frequency for (a) ethane oxidation and (b) ethylene oxidation on 0.1 g Ni/HY (in solid circles) and 0.1 g Ni/KY (in open circles) catalysts, respectively.

by the carbon balance for ethylene and CO_x. As expected for coking, CO_2 was detected after purging the reactor with He and introducing O_2.

3.4. Extended X-ray absorption fine structure (EXAFS) study

EXAFS measurements were performed to obtain data on the oxidation states and bonding modalities in Ni-loaded zeolites. Fig. 10 shows the Fourier transformation of k^2-weighted EXAFS [$k^{2*}\chi(k)$] of as-prepared NiY, Ni/HY, Ni metal, and NiO samples. Based on the known crystal structure of Ni metal (FCC) and NiO (rocksalt), the peaks at 1.65 Å (peak *a* in Fig. 10) and 2.58 Å (peak *c*) can be assigned to Ni–O bonds with a bond length of 2.09 Å and Ni···Ni pairs at a distance of 2.95 Å, respectively. The peak in the Ni metal spectrum at 2.18 Å (peak *b*) is due to Ni–Ni bonds with a bond length of 2.49 Å. From Fig. 10, it is apparent that peak *a* is present in the NiY spectrum, while peaks *b* and *c* are absent, indicating that Ni^{2+} is attached to an O atom of the zeolite framework. Ni/HY gives a strong *b* peak, indicating that Ni–Ni bonds form after reduction by H_2, and Ni metal particles may be present on the zeolite support, however, since there is still evidence for peak *a*, it appears that not all the Ni^{2+} has been reduced in the Ni/HY sample.

Fig. 11 shows the Fourier transformation of k^2-weighted EXAFS of Ni/HY catalyst treated with flowing reactant gas at various temperatures. The presence of both peaks *a* and *b* indicates that, during the ODHE catalytic process, Ni is present in particles containing both Ni–Ni and Ni–O bonds. The appearance of peak *c* indicates that O is present not only on the surface of metal particles, but also inside the particles. Peaks *a* and *c* increase with temperature, while peak *b* decreases with temperature, corresponding to an increasing number of Ni–O bonds and a decreasing number of Ni–Ni bonds. This result demonstrates that at higher reaction temperatures the catalyst contains more Ni in a higher oxidation state than metallic Ni. The appearance of peak *c* at higher temperatures (>500 °C) indicates that O_2 oxidizes Ni clusters to give NiO. This change is consistent with reducible transition metals undergoing the Mars van Krevelen mechanism [2,74]. EXAFS spectra of Ni and NiO were used as standards to fit the EXAFS spectra of the Ni/HY catalyst treated with the reactant gas flow at different temperatures to determine that the contribution of oxidized Ni to the overall Ni components on Ni/HY increased with the treatment temperature (see Table 3). For example, NiO has a 69.6% contribution at 450 °C and 90.2% contribution at 600 °C. A similar result was obtained from the Fourier transform spectrum of k^2-EXAFS of Cu/HY (Fig. 12) treated with the reactant gas flow at 500 and 600 °C.

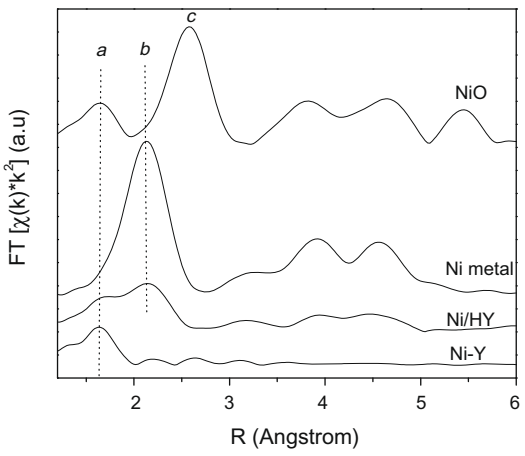

Fig. 10. Fourier transformed spectra of k^2-weighted EXAFS for NiY, Ni/HY, Ni metal foil, and NiO, as indicated.

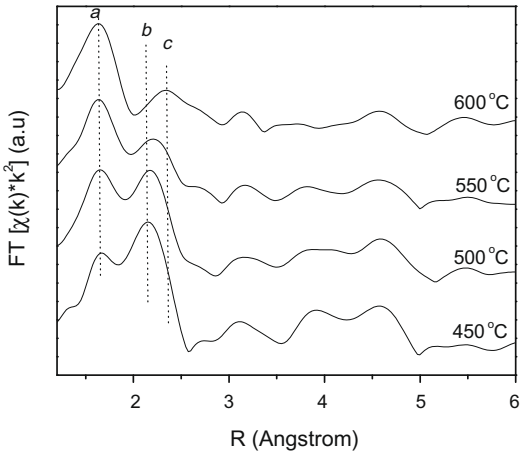

Fig. 11. Fourier transformed spectra of k^2-weighted EXAFS (not corrected for phase shifts) of 0.1 g Ni/HY treated in a flow of 9.7 ml/min C_2H_6 + 3.3 ml/min O_2 + 62 ml/min He for 1 h at the temperature as specified.

Table 3
Metal/metal oxide(s) contributions to the overall metal components for Ni/HY and Cu/HY treated with reactant gas flow as a function of temperature.

T (°C)	Ni (%)	NiO (%)
Ni/HY		
450	30.4	69.9
500	21.6	78.4
550	15.5	84.5
600	9.8	90.2
	Cu_2O (%)	CuO (%)
Cu/HY		
500	12.0	88.0
600	6.6	93.4

The results of fitting the k^2-EXAFS of the treated Cu/HY, using Cu, Cu_2O and CuO as standards, are presented in the lower part of Table 3: CuO contributes 88% at 500 °C, and 93.4% at 600 °C to the overall Cu components on Cu/HY.

3.5. ODHE reaction mechanism

At this point it is useful to summarize the reaction mechanisms proposed in the literature for ODHE [2,19,73–77]. These proposed

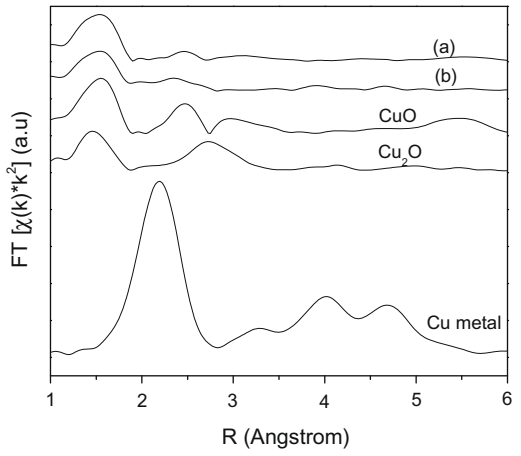

Fig. 12. Fourier transformation spectra of k^2-weighted EXAFS of Cu metal, Cu_2O, CuO, and 0.1 g Cu/HY treated with the reactant flow for 1 h at (a) 500 °C and (b) 600 °C.

mechanisms and the associated kinetic modeling have been mainly applied to V- and Mo-based catalysts. Generally accepted mechanisms for the oxidation of hydrocarbons over reducible metal oxide catalysts are the Mars van Krevelen (MK) or the ER-SSAM mechanism [2,74]. The metals examined in this work, Ni, Cu, and Fe catalysts are also reducible transition metals. Kung [74] suggested that rupture of the first C–H bond is generally the slowest step in the ODH reaction, and that the activation of the C–H bond by a metal oxide leads to the formation of alkyl or alkoxide species. However, the high reactivity of surface intermediates has made direct observation of these species difficult, and the detailed reaction mechanism for light alkane oxidation remains elusive. Nevertheless, existing experimental data suggest two types of pathways for ODHE:

(A) C_2H_6 reacts with surface oxides to form a metal-ethoxide and a surface hydroxyl,

$$C_2H_6 + 2M{-}O \rightarrow C_2H_5{-}O{-}M + M{-}O{-}H. \quad (3)$$

The metal ethoxide may then undergo two possible reactions: α-hydrogen abstraction or β-hydrogen abstraction, which lead to an aldehyde or C_2H_4, respectively

$$CH_3CH_2{-}O{-}M \rightarrow CH_3{-}CHO + M{-}H \quad (4)$$
$$CH_3CH_2{-}O{-}M \rightarrow CH_2{=}CH_2 + M{-}O{-}H \quad (5)$$

(B) C_2H_6 reacts with surface oxides to form a ethyl–metal complex followed by β-hydrogen elimination to give C_2H_4 and a metal-hydride site,

$$C_2H_6 + M{-}O + M \rightarrow C_2H_5{-}M + M{-}O{-}H \quad (6)$$
$$C_2H_5{-}M \rightarrow C_2H_4 + M{-}H \quad (7)$$

After the reactions in either pathways (A) and (B) take place, surface hydroxyl and/or surface hydrogen may undergo the following reactions to produce a reduced metal site and water:

$$M{-}H + M{-}O \rightarrow M + M{-}O{-}H \quad (8)$$
$$M{-}H + M{-}O{-}H \rightarrow 2M + H_2O \quad (9)$$
$$2M{-}O{-}H \rightarrow M{-}O + M + H_2O \quad (10)$$

Oxidation of the reduced metal site by O_2 then regenerates the oxidized metal site, completing the catalytic cycle:

$$M + 1/2O_2 \rightarrow M{-}O \quad (11)$$

These results provide several clues that suggest that mechanism (A) is more plausible than mechanism (B), at least for the systems studied. Firstly, the C–H bond activation step in mechanism (A) requires two oxidized sites, while an oxidized site and a reduced site are needed in mechanism (B). The EXAFS data show that a higher ratio of oxidized sites over reduced sites at higher temperatures correlates with an increase in C_2H_4 selectivity with temperature. These results are consistent with a greater percentage of oxidized sites leading to an increased C_2H_4 selectivity. Nakamura and coworkers found that C_2H_6 conversion decreases by ~20% at 600 °C and selectivity decreases to nearly zero on NiO/MgO, when H_2 reduction was carried out before the reaction [40]. Secondly, IR spectroscopic evidence provided by Busca and coworker [78] indicates that C–H bond rupture leads to the formation of alkoxides, for both the total oxidation and the oxidative dehydrogenation of propane and butane on Mn_3O_4, Co_3O_4, and $MgCr_2O_4$. Additionally, a Brønsted acid site can catalyze the β-hydrogen abstraction step as depicted in Scheme 1. Taken together, these data are suggestive of pathway (A) being more likely than pathway (B) for ODHE over a Ni/HY catalyst. Our data also suggest that Brønsted acid sites favor ($k_1 + k_2$) and disfavor k_3 (see Eq. (2)) and that the decrease in k_3 relative to ($k_1 + k_2$) is not due to a higher desorption rate of C_2H_4 on reduced Ni.

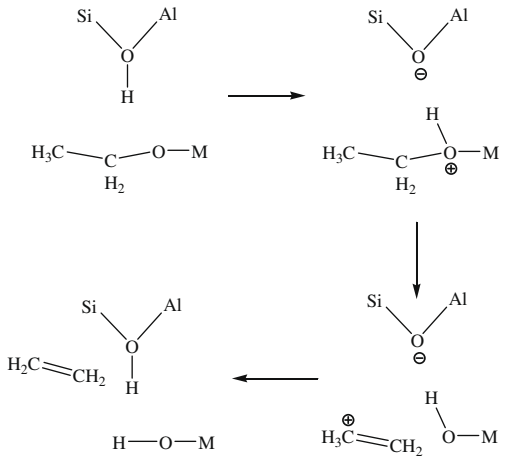

Scheme 1. β-Hydrogen abstraction reaction of metal ethoxide to form C_2H_4 catalyzed by a zeolitic acid site.

4. Conclusion

(1) Transition metal (Ni, Cu, and Fe) loaded acidic and basic Y zeolites were synthesized and characterized, and their catalytic performance for ODHE was examined. Both the ODHE activity and the C_2H_4 selectivity on these metal-loaded Y zeolites follow the trend Ni > Cu > Fe. Ni/HY has a productivity of C_2H_4 of 1.08 $g_{C_2H_4}\ g_{cat}^{-1}\ h^{-1}$ and a C_2H_4 selectivity of ~75% at 600 °C.

(2) For all three metals studied, both high ethane conversion and C_2H_4 selectivity were favored by an acidic zeolite support.

(3) Zeolite acidity leads to a relatively larger rate constant for ethane oxidation ($k_1 + k_2$) as compared to ethylene oxidation (k_3) on Ni-loaded Y zeolite. The ratio, $k_3/(k_1 + k_2)$, decreases with temperature for both Ni/KY and Ni/HY, which correlates with an increase in C_2H_4 selectivity with temperature.

(4) EXAFS shows that during ODHE on Ni/HY, Ni is present in particles containing both Ni–Ni and Ni–O bonds, and oxygen is present both on the metal particle surface and in the lattice shell. Further, the ratio of oxidized Ni over metallic Ni increases with temperature.

(5) Overall, our data provide clues that suggest that mechanism (A), which involves the formation of metal ethoxides and subsequent β-H abstraction to form C_2H_4, is more likely than mechanism (B) for the ODHE reaction catalyzed by Ni-loaded Y zeolite.

Acknowledgments

This work was supported by the Chemical Sciences, Geosciences and Biosciences Division, Office of Basic Energy Sciences, Office of Science, US Department of Energy (DE-FG02-03- ER15457), at the Northwestern University Institute for Catalysis in Energy Processes. Portions of this work were performed at the DuPont-Northwestern-Dow Collaborative Access Team (DND-CAT) located at Sector 5 of the Advanced Photon Source (APS). DND-CAT is supported by E.I. DuPont de Nemours & Co., The Dow Chemical Company and the State of Illinois. Use of the APS was supported by the U. S. Department of Energy, Office of Science, Office of Basic Energy Sciences, under Contract No. DE-AC02-06CH11357. This work made use of the J.B. Cohen X-ray Facility supported by the MRSEC

program of the National Science Foundation (DMR-0520513) at the Materials Research Center of Northwestern University.

References

[1] F. Cavani, N. Ballarini, A. Cericola, Catal. Today 127 (2007) 113.
[2] J.F. Brazdil, Top. Catal. 38 (2006) 289.
[3] L. Ćapek, J. Adam, T. Grygar, R. Bulánek, L. Vradman, G. Košová-Kučerová, P. Čičmanec, P. Knotek, Appl. Catal. A 342 (2008) 99.
[4] P. Botella, A. Dejoz, J.M. Lopez Nieto, P. Concepcion, M.I. Vazquez, Appl. Catal. A 298 (2006) 16.
[5] M.V. Martınez-Huerta, X. Gao, H. Tian, I.E. Wachs, J.L.G. Fierro, M.A. Banares, Catal. Today 118 (2006) 279.
[6] E. Heracleous, M. Machli, A.A. Lemonidou, I.A. Vasalos, J. Mol. Catal. A 232 (2005) 29.
[7] L. Lisi, G. Ruoppolo, M.P. Casaletto, P. Galli, M.A. Massucci, P. Patrono, F. Pinzari, J. Mol. Catal. A 232 (2005) 127.
[8] M.P. Casaletto, L. Lisi, G. Mattogno, P. Patrono, G. Ruoppolo, Appl. Catal. A 267 (2004) 157.
[9] M.P. Casaletto, L. Lisi, G. Mattogno, P. Patrono, F. Pinzari, G. Ruoppolo, Catal. Today 91/92 (2004) 271.
[10] P. Concepcion, M.T. Navarro, T. Blasco, J.M. Lopez Nieto, B. Panzacchi, F. Rey, Catal. Today 96 (2004) 179.
[11] Z.-S. Chao, E. Rckenstein, J. Catal. 222 (2004) 17.
[12] P. Concepcion, T. Blasco, J.M. Lopez Nieto, A. Vidal-Moya, A. Martınez-Arias, Micropor. Mesopor. Mater. 67 (2004) 215.
[13] B. Solsona, V.A. Zazhigalov, J.M. López Nieto, I.V. Bacherikova, E.A. Diyuk, Appl. Catal. A 249 (2003) 81.
[14] L. Lisi, P. Patrono, G. Ruoppolo, J. Mol. Catal. A 204 (2003) 609.
[15] B. Solsona, T. Blasco, J.M. Lopez Nieto, M.L. Penã, F. Rey, A. Vidal-Moya, J. Catal. 203 (2001) 443.
[16] P. Concepcion, J.M. Lopez Nieto, Catal. Commun. 2 (2001) 363.
[17] T. Blasco, A. Galli, J.M. Lopez Nieto, F. Trifirò, J. Catal. 169 (1997) 203.
[18] P. Concepcion, A. Corma, J.M. Lopez Nieto, J. Perez Pariente, Appl. Catal. A 143 (1996) 17.
[19] G. Tsilomelekis, A. Christodoulakis, S. Boghosian, Catal. Today 127 (2007) 139.
[20] A. Christodoulakis, E. Heracleous, A.A. Lemonidou, S. Boghosian, J. Catal. 242 (2006) 16.
[21] B. Solsona, A. Dejoz, T. Garcia, P. Concepcion, J.M. Lopez Nieto, M.I. Vazquez, M.T. Navarro, Catal. Today 117 (2006) 228.
[22] C. Liu, U.S. Ozkan, J. Mol. Catal. 220 (2004) 53.
[23] R.B. Watson, S.L. Lashbrook, U.S. Ozkan, J. Mol. Catal. A 208 (2004) 233.
[24] G. Grubert, E. Kondratenko, S. Kolfa, M. Baerns, P. van Geem, R. Parton, Catal. Today 81 (2003) 337.
[25] R.B. Watson, U.S. Ozkan, J. Catal. 208 (2002) 124.
[26] G.D. Claycomb, P.M.A. Sherwood, B.E. Traxel, K.L. Hohnet, J. Phys. Chem. C 111 (2007) 18724.
[27] E.A. de Graaf, G. Rothenberg, P.J. Kooyman, Appl. Catal. A 278 (2005) 187.
[28] A.S. Bodke, D. Henning, L.D. Schmidt, S.S. Bharadwaj, J.J. Maj, J. Sidddall, J. Catal. 191 (2000) 62.
[29] A.S. Bodke, D.A. Olschki, L.D. Schmidt, E. Ranzi, Science 285 (1999) 712.
[30] D.W. Flick, M.C. Huff, Appl. Catal. A 187 (1999) 13.
[31] C. Yokoyama, S.S. Bharadwaj, L.D. Schmidt, Catal. Lett. 38 (1996) 181.
[32] T. Osawa, P. Ruiz, B. Delmon, Catal. Today 61 (2000) 309.
[33] M. Roussel, M. Bouchard, K. Karim, S. Al-Sayari, E. Bordes-Richard, Appl. Catal. A 308 (2006) 62.
[34] B. Solsona, A. Dejoz, T. Garcia, P. Concepcion, J.M. Lopez Nieto, M.I. Vazquez, M.T. Navarro, Catal. Today 117 (2006) 228.
[35] Q. Xie, L. Chen, W. Weng, H. Wan, J. Mol. Catal. A 240 (2005) 191.
[36] R.B. Watson, U.S. Ozkan, J. Catal. 191 (2000) 12.
[37] P. Botella, E. García-González, A. Dejoz, J.M. López Nieto, M.I. Vázquez, J. González-Calbet, J. Catal. 225 (2004) 428.
[38] J.M. López Nieto, P. Botella, P. Concepción, A. Dejoz, M.I. Vázquez, Catal. Today 91/92 (2004) 241.
[39] E. Heracleous, A.A. Lemonidou, J. Catal. 237 (2006) 162.
[40] K.-I. Nakamura, T. Miyake, T. Konishi, T. Suzuki, J. Mol. Catal. A 260 (2006) 144.
[41] E. Heracleous, A.A. Lemonidou, J. Catal. 237 (2006) 175.
[42] E. Heracleous, A.F. Lee, K. Wilson, A.A. Lemonidou, J. Catal. 231 (2005) 159.
[43] X. Zhang, J. Liu, Y. Jing, Y. Xie, Appl. Catal. A 240 (2003) 143.
[44] X. Zhang, Y. Gong, G. Yu, Y. Xie, J. Mol. Catal. A 180 (2002) 293.
[45] Y. Schuurman, V. Ducarme, T. Chen, W. Li, C. Mirodatos, G.A. Martin, Appl. Catal. A. 163 (1997) 227.
[46] K. Sun, H. Xia, Z. Feng, R. van Santen, E. Hensen, C. Li, J. Catal. 254 (2008) 383.
[47] I. Yuranov, D.A. Bulushev, A. Renken, L. Kiwi-Minsker, Appl. Catal. A. 319 (2007) 128.
[48] N.R. Shiju, S. Fiddy, O. Sonntag, M. Stockenhuber, G. Sankar, Chem. Commun. 47 (2006) 4955.
[49] E.J.M. Hensen, Q. Zhu, R.A. van Santen, J. Catal. 233 (2005) 136.
[50] A. Waclaw, K. Nowinska, W. Schwieger, Appl. Catal. A 270 (2004) 151.
[51] J.F. Jia, K.S. Pillai, W.M.H. Sachtler, J. Catal. 221 (2004) 119.
[52] A. Ribera, I.W.C.E. Arends, S. de Vries, J. Perez-Ramirez, R.A. Sheldon, J. Catal. 195 (2000) 287.
[53] L.M. Kustov, A.L. Tarasov, V.I. Bogdan, A.A. Tyrlov, J.W. Fulmer, Catal. Today 61 (2000) 123.
[54] K. Yoshizawa, Y. Shiota, T. Yumura, T. Yamabe, J. Phys. Chem. B 104 (2000) 734.
[55] A. Held, J. Kowalska, K. Nowinska, Appl. Catal. B 64 (2006) 201.
[56] J. Perez-Ramirez, A. Gallardo-Llamas, J. Phys. Chem. B 109 (2005) 20529.
[57] J. Perez-Ramirez, A. Gallardo-Llamas, Appl. Catal. A 279 (2005) 117.
[58] A. Gallardo-Llamas, C. Mirodatos, J. Perez-Ramirez, Ind. Eng. Chem. Res. 44 (2005) 455.
[59] J. Perez-Ramirez, A. Gallardo-Llamas, J. Catal. 223 (2004) 382.
[60] K. Nowinska, A. Waclaw, A. Izbinska, Appl. Catal. A 243 (2003) 225.
[61] A.V. Kucherov, V.D. Nissenbaum, T.N. Kucherova, L.M. Kustov, Kinet. Catal. 43 (2002) 99.
[62] S. Bhatia, in: Zeolite Catalysis: Principles and Applications, CRC Press Inc., Florida, 1990, p. 116.
[63] W.M.H. Sachtler, Acc. Chem. Res. 26 (1993) 383.
[64] C. Dossi, R. Psaro, R. Ugo, Z.C. Zhang, W.M.H. Sachtler, J. Catal. 149 (1994) 92.
[65] R.A. Dalla Betta, M. Boudart, in: H. Hightower (Ed.), Proceeding of the 5th International Congress on Catalysis, Elsevier, Amsterdam, 1973, p. 1329.
[66] S.T. Homeyer, Z. Karpiński, W.M.H. Sachtler, J. Catal. 123 (1990) 60.
[67] K. Suzuki, N. Katada, M. Niwa, J. Phys. Chem. C (111) (2007) 894.
[68] E.A. Stern, W.T. Elam, B.A. Bunker, K.Q. Lu, S.M. Heald, Nucl. Instrum. Methods Phys. Res. 195 (1982) 345.
[69] B. Ravel, M. Newville, J. Synchrotron Radiat. 12 (2005) 537.
[70] B.-Z. Zhan, E. Iglesia, Angew. Chem., Int. Ed. 46 (2007) 3697.
[71] P.A. Wright, in: Microporous framework solid, RSC, Cambridge, 2008 (Chapter 8).
[72] C.Y. Kao, K.T. Huang, B.Z. Wan, Ind. Eng. Chem. Res. 33 (1994) 2066.
[73] M.D. Argyle, K. Chen, A.T. Bell, E. Iglesia, J. Phys. Chem. B 106 (2002) 5421.
[74] H.H. Kung, Adv. Catal. 40 (1994) 1.
[75] F. Klose, M. Joshi, C. Hamel, A. Seidel-Morgenstern, Appl. Catal. A 260 (2004) 101.
[76] E. Heracleous, A.A. Lemonidou, J.A. Lercher, Appl. Catal. A 264 (2004) 73.
[77] F. Cavani, F. Trifirò, Catal. Today 51 (1999) 561.
[78] G. Busca, E. Finocchio, V. Lorenzelli, G. Ramis, M. Baldi, Catal. Today 49 (1999) 453.